Journal of Geophysical Research: Solid Earth

RESEARCH ARTICLE
10.1029/2018JB016336

Key Points:
- Locked asperities on subduction megathrusts cause slip deficit to accumulate in regions that would otherwise slide at the convergence rate
- Unruptured locked zones restrict the maximum magnitude of slip in earthquakes that rupture adjacent sections of the plate boundary
- Modeled patterns of interseismic deformation near the trench are compatible with tsunami-related coseismic observations

Supporting Information:
- Supporting Information S1
- Data Set S1
- Data Set S2
- Data Set S3
- Data Set S4

Correspondence to:
M. W. Herman,
m.w.herman@uu.nl

Citation:
Herman, M. W., Furlong, K. P., & Govers, R. (2018). The accumulation of slip deficit in subduction zones in the absence of mechanical coupling: Implications for the behavior of megathrust earthquakes. *Journal of Geophysical Research: Solid Earth*, *123*, 8260–8278. https://doi.org/10.1029/2018JB016336

Received 5 JUL 2018
Accepted 29 AUG 2018
Accepted article online 7 SEP 2018
Published online 26 SEP 2018

The Accumulation of Slip Deficit in Subduction Zones in the Absence of Mechanical Coupling: Implications for the Behavior of Megathrust Earthquakes

Matthew W. Herman[1,2], Kevin P. Furlong[1], and Rob Govers[2]

[1]Department of Geosciences, Pennsylvania State University, University Park, PA, USA, [2]Department of Earth Sciences, Utrecht University, Utrecht, Netherlands

Abstract The distribution of slip during subduction megathrust earthquakes depends on the slip deficit that accumulates on the plate interface prior to the event. We develop 3-D finite element models of subduction zones to investigate how locked zones restrict surrounding regions on the plate boundary from sliding. What is new is that we quantify the slip around asperities on the megathrust. The models show plate interface slip increasing from zero at the edge of a locked zone to the relative plate motion over a distance of ~200 km along the megathrust. This area of reduced slip accumulates a seismic moment deficit up to 10 times larger than the moment deficit in the asperity alone. Updip of locked areas, slip at the trench can be reduced by more than 50% of the plate motion. Despite large displacements of the upper plate near the trench, this region moves as a semirigid block. Rupture models of the 2011 Tohoku earthquake, its tsunami characteristics, and geophysical observations near the trench can be interpreted to reflect the consequences of slip deficit accumulated on a low friction interface updip of the seismogenic zone. Neighboring asperities affect plate interface slip in a nonlinear way. Multiple asperities have overlapping pseudo-coupled regions that may restrict the magnitude of coseismic slip in single-asperity ruptures. Once an earthquake has a rupture length greater than ~250 km, it may recover the entire accumulated slip deficit. This is consistent with the magnitude of coseismic slip in several recent great megathrust earthquakes.

1. Introduction

The amount and distribution of slip deficit that accumulates on the plate boundary prior to an earthquake are important to the potential kinematic characteristics of great (moment magnitude Mw 8.0+) subduction plate interface (megathrust) ruptures. Frictionally locked areas (asperities) accumulate slip deficit at the convergence rate, while other sections of the interface sufficiently far from these asperities accumulate zero slip deficit; that is, they slide, creep, or otherwise deform at or near the relative plate velocity. There are also sections of subduction plate interfaces that move at velocities slower than the convergence rate during the interseismic period. One cause of these reduced velocities arises from the continuity of the plates; regions on the plate boundary that would otherwise creep will slide more slowly when they are sufficiently close to a locked zone. We quantify the pattern of inter-seismic slip deficit produced by this effect to improve estimates of slip deficit accumulation over the plate boundary and evaluate how it can also affect the patterns of coseismic slip in great earthquakes.

Figure 1 shows the relationship between coseismic slip and the estimated accumulation of interseismic slip deficit (derived from geodetic measurements) for four recent great earthquakes along well instrumented subduction zones (Figures 1a–1c show events offshore Chile: (a) 2014 Mw 8.2 Iquique, (b) 2015 Mw 8.3 Illapel, and (c) 2010 Mw 8.8 Maule, and Figure 1d shows the 2011 Mw 9.0 Tohoku event offshore Japan). The locations of dominant moment release in these events are assumed to correspond to asperities—areas that are locked between earthquakes. The locations of peak coseismic slip in these events are generally in or near regions inferred to be accumulating slip deficit at 80% or more of the convergence rate. It should be noted that both the 2010 Maule and 2011 Tohoku earthquakes also had areas of high coseismic slip in regions inferred to be accumulating interseismic slip deficit at a lower rate (Figures 1c and 1d). In all four of these earthquakes, smaller but still significant amounts of coseismic slip extend away from the regions of peak slip along-strike or updip into areas of inferred lower accumulated slip deficit surrounding the asperities. Sometimes a rupture will propagate from one asperity to another across one of these low slip deficit

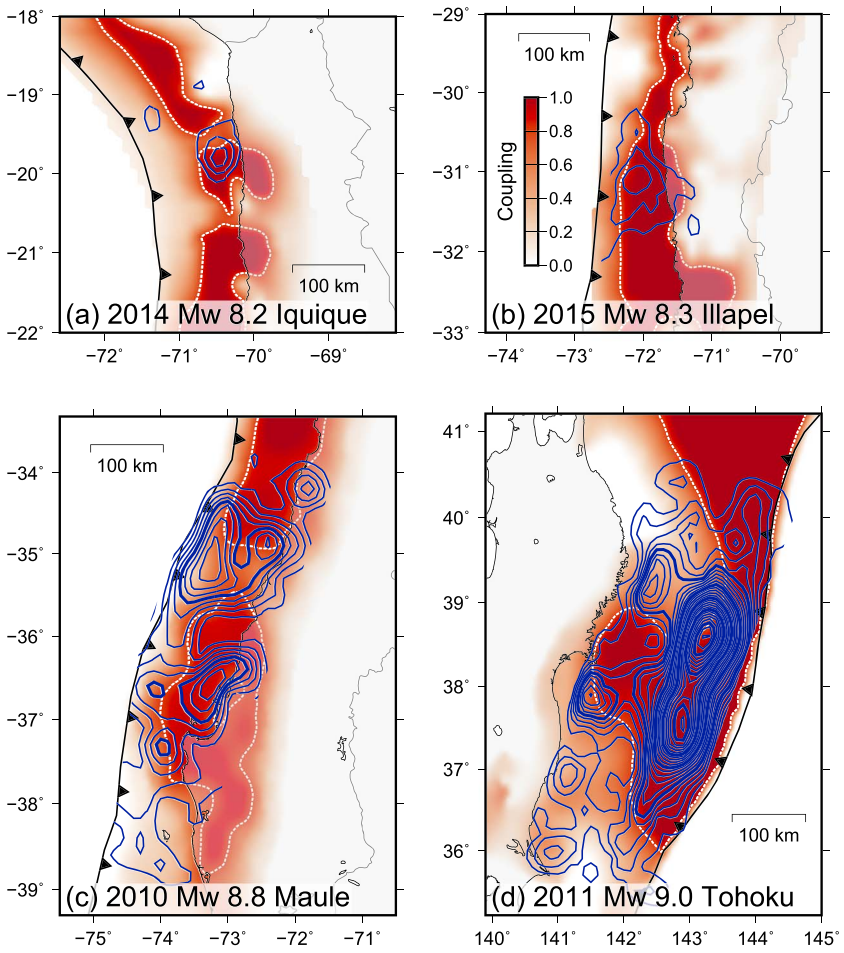

Figure 1. Comparisons of pre-earthquake megathrust slip deficit accumulation with coseismic slip distributions (Hayes, 2017). Interseismic coupling is indicated by the background colors, and the dashed white line is the 0.8 coupling contour. The thin blue lines are 2-m coseismic slip contours, and the bold blue lines are 10-m slip contours. (a) 2014 Mw 8.2 Iquique, Chile, earthquake (coupling distribution from Metois et al., 2016); (b) 2015 Mw 8.3 Illapel, Chile, earthquake (coupling from Metois et al., 2016); (c) 2010 Mw 8.8 Maule, Chile, earthquake (coupling from Moreno et al., 2010); (d) 2011 Mw 9.0 Tohoku, Japan, earthquake (coupling from Loveless & Meade, 2011).

regions. This may lead to substantial coseismic slip involving multiple asperities during a single event, as occurred in the 2010 Maule or 2011 Tohoku earthquakes. These largest events have both greater rupture areas involving multiple asperities and larger slip magnitudes within each asperity as compared to relatively smaller, single-asperity earthquakes (e.g., the 2014 Iquique and 2015 Illapel events).

The large tsunamis generated during the Illapel, Maule, and Tohoku earthquakes are also consistent with substantial coseismic slip on the shallow part of the subduction megathrust, seen in some of the rupture models of these events (Figures 1b–1d). The occurrence of substantial shallow coseismic slip implies that this part of the plate interface accumulated significant slip deficit prior to these great earthquakes. However, the shallow part of the subduction megathrust does not appear to be frictionally locked in the same way as deeper parts of the plate interface, based on differences in the seismic waves radiated from these regions (Lay et al., 2012). In addition, earthquakes rarely initiate at shallow depths. The seismogenic zone on the megathrust, defined as the depth range where earthquakes nucleate, typically lies at depths of 15–45 km in subduction zones (Hayes et al., 2012; Pacheco et al., 1993). Therefore, shallow slip deficit accumulates despite apparent physical characteristics that differ from the seismogenic section of the plate interface.

In this study, we use elasto-static models with rheologically simplified locking on the plate interface to (a) understand and quantify the inter-seismic partial slip deficit around asperities accumulating slip deficit at or near the convergence rate, (b) compare the results with megathrust locking observations, and (c)

provide insight into the causes of observations of coseismic slip in great subduction zone earthquakes. One approach toward understanding the range of coseismic slip behaviors applies dynamic simulations of earthquake cycles with mechanical, rheological, and frictional complexity (e.g., Avouac, 2015; Hashimoto et al., 2014; Kaneko et al., 2010; Liu & Rice, 2005; Thomas et al., 2014; van Dinther et al., 2013). Although these models can reproduce many features of the earthquake cycle across timescales, their complexity obscures the primary contributor to interseismic geodetic observations and the corresponding implications for coseismic rupture scenarios. In this study, we specifically investigate the effect of elasticity in the plates on the pattern of slip on the plate boundary.

Our modeling approach is based on the observation that the seismogenic section of the megathrust is embedded in a region that generally behaves elastically (Turcotte & Schubert, 2002). This implies that deformation in each plate should be continuous away from the asperity. As a consequence, sections of the fault that would otherwise slide or creep will have lower slip if they are near a locked patch. This effect decreases with distance from the locked patch in a way that has not been previously quantified. When imaged geodetically, the transition zone between locked and fully sliding sections of the megathrust will appear to be "partially coupled," even if this region is otherwise able to slide at the plate motion velocity in the absence of the nearby asperity (Wang & Dixon, 2004). We refer to this type of reduced inter-seismic slip adjacent to an asperity as "pseudo-coupling" to distinguish it from (partial) slip deficit produced by mechanical coupling (such as friction) on the interface.

Pseudo-coupling has been inferred along the strike-slip Hayward fault system in California, where analyses of interseismic GPS and creepmeter observations indicate that sections of the fault are creeping at a rate slower than the far-field relative velocity (Gans et al., 2003; Malservisi et al., 2003). These studies modeled the pattern of observed surface displacements with a fault consisting of a binary distribution of fully locked asperities on an otherwise zero-resistance interface. The combined asperity and surrounding partial slip region reflect a larger potential coseismic slip area than might be estimated based on the distribution of fully coupled asperities alone. These studies concluded that the slip deficit over the entire Hayward fault (including both locked and creeping sections sliding at lower velocities) is accommodated dominantly through large earthquakes. Bürgmann et al. (2005) applied this concept to the Kamchatka subduction zone, showing that interseismic upper plate GPS velocities are well matched by a distribution of fully locked areas (corresponding to the high-slip regions of previous large earthquakes) surrounded by a frictionless interface that is prevented from sliding by the asperities. Almeida et al. (2018) also used this approach to show that the area updip of a locked zone can accumulate significant slip deficit, although onshore geodetic data may not be able to observe the effects of this slip distribution.

A similar result was derived by Hetland and Simons (2010) for slip deficit accumulation around an asperity on a subduction megathrust through a conceptually different model. They drove their simulations with earthquakes that triggered postseismic creep on the surrounding interface and recognized that the total slip at every point on the plate interface should be the same over an earthquake cycle. This led to regions with high postseismic creep near the asperity having lower levels of inter-seismic slip; that is, these areas would be interpreted as accumulating high slip deficit late in the interseismic stage of the earthquake cycle.

We model the effects of relative plate motion and locking in the interseismic period using a numerical modeling approach, similar to Gans et al. (2003) and Malservisi et al. (2003). This approach allows us to investigate interactions between locked and unlocked regions on the plate interface under geologically representative boundary conditions, explore the effects of geometric and rheologic complexity, and constrain the potential effects on megathrust earthquakes.

2. Model Setup

We use a simplified subduction zone model setup that allows us to isolate the effects of pseudo-coupling independent of other geometric complexity (e.g., interface dip or curvature and asperity shape; Figure 2). The subducting plate is a planar slab with a 25° dip. The upper plate is triangular in cross section, extending 400 km horizontally from the trench to a "backstop" (the *x* direction; Govers et al., 2018) and 1,000 km along strike (*y* direction). Because we are assessing the spatial deformation pattern caused by megathrust locking, we represent cumulative relative plate motion in the interseismic stage with displacement boundary conditions. We apply 1-m displacements to both the updip and downdip sides of the subducting plate (arrows in

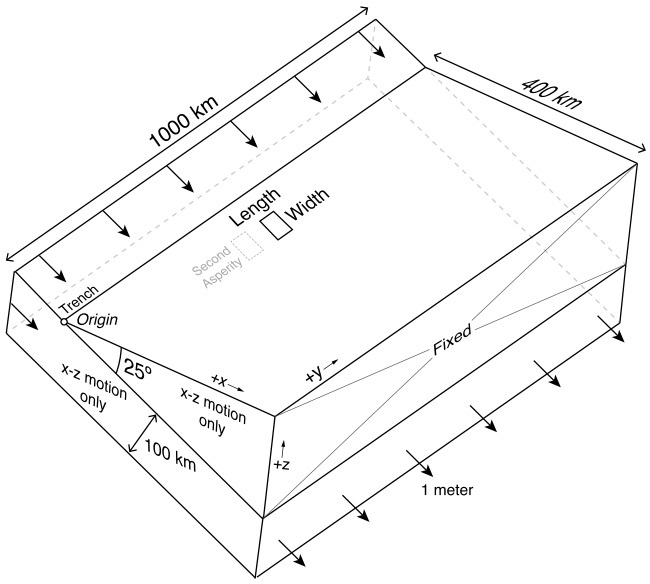

Figure 2. Subduction model setup. The subducting slab is planar and dips at 25°. It is displaced parallel to the dip direction by 1 m at both ends (indicated by arrows), while the upper plate backstop is held fixed and the sides are constrained to move only in the *x-z* plane. All points on the interface between upper and subducting plates are allowed to slide with no resistance except for the nodes within rectangular locked zones with dimensions *Length* (along strike) and *Width* (along dip). In these regions the plates cannot slide.

Figure 2), while the backstop of the upper plate is held fixed in all directions. The along-strike sides of the model are constrained to move only in the *x-z* plane. We assign homogeneous elastic properties to the two plates (Young's modulus = 100 GPa and Poisson's ratio = 0.25, corresponding to shear modulus = 40 GPa). Since the system is elastic, the modeled displacements, strains, and stresses scale linearly with the amount of relative displacement (or displacement rate), assuming that the model geometry is held constant. The specific choices of elastic moduli do not affect the modeled displacements (only the associated stress levels), because our model is driven by displacements and not forces. Three-dimensional meshes are generated with Gmsh (Geuzaine & Remacle, 2009) and convergence tests demonstrate that our results are insensitive to further mesh refinement. We use the finite element modeling platform GTECTON (version 2017.1; Govers & Wortel, 1993; Govers & Wortel, 2005; Govers et al., 2018) compiled with PETSc 3.4.2 (http://www.mcs.anl.gov/petsc) to solve the static mechanical equilibrium equations.

Two types of boundary conditions are imposed on the plate interface: locked (i.e., zero slip allowed) and unlocked (i.e., free to slide with no resistance). We define locked sections as rectangular areas on the megathrust with one side oriented parallel to strike (the along-strike dimension is the fault length) and the other along dip (the fault width) for straightforward comparison with the solutions of Okada (1992; Figure 2). We also tested circular and elliptical locked zones and found that the model results show limited sensitivity to the exact shape of the locked zone. Any area outside a locked section on the surface is made free to slide using the "slippery node" formulation, which allows nodes on the interface to have discontinuous displacements in the plane of the fault (Melosh & Williams, 1989). These dynamically slipping areas of the megathrust are defined to have zero shear traction resolved on the interface.

Studies of the effects of shear tractions acting along subduction plate boundaries suggest that a low shear resistance boundary condition outside asperities is a reasonable approximation over the decades- to centuries-long time scales of inter-seismic loading. The regions updip and immediately downdip of the seismogenic zone on the megathrust are thought to be both frictionally weak and sliding stably (Hardebeck, 2015; Ikari et al., 2011; Scholz, 1998), while the regions farther downdip on the megathrust boundary are envisioned to be narrow shear zones creeping continuously at reduced shear stresses due to higher temperatures and viscous rheology (Hyndman et al., 1997; Tichelaar & Ruff, 1993; van Keken et al., 2002). We also define regions outside of locked areas, within the seismogenic depth range, as having zero shear traction (Hardebeck & Loveless, 2017) and sliding stably, although it is unknown whether these areas exhibit this behavior because of mineralogy (Saffer & Marone, 2003), high fluid pressures (Audet et al., 2009), interface topography and geometry (Wang & Bilek, 2014), or other processes. It should be noted that other studies have interpreted these regions as sliding stably at high shear tractions (e.g., Gao & Wang, 2014). Applying zero shear tractions to the unlocked areas in our models results in the minimum amount of interseismic slip deficit that can accumulate in those locations; a higher shear resistance would increase the slip deficit. In our analyses, we also test the effects of choosing different resistive forces on the plate interface in our models.

We investigate models for several simple asperity configurations that are representative of locking patterns inferred in subduction zones (e.g., those shown in Figure 1). We explore the effects of individual asperity size and location as well as slab dip on the accumulation of slip deficit on the plate interface. We also evaluate the effects on displacements and stresses throughout the model volume. We pay particular attention to displacements on the surface of the upper plate because these are analogous to geodetic observations. The model setup allows us to define an arbitrary number of locked regions with varying dimensions on the interface (Figure 2). We evaluate how nearby asperities may interact with each other in the interseismic and coseismic stages by placing multiple locked areas on the interface. The underlying physical character of asperities with

different dimensions appears to be similar based on earthquake characteristics (Ide & Beroza, 2001; Kanamori & Anderson, 1975), so we treat all of these locked zones identically in our models.

3. Results

3.1. Single Asperity (Reference Model)

3.1.1. Fault Slip

The reference model contains a 40 km by 40 km locked zone (the dimensions of a Mw ~7.3 earthquake; Mai & Beroza, 2000; Allen & Hayes, 2017; and the approximate length scale that can be resolved in slip inversions using onshore geodetic data) centered at a depth of 30 km (Figure 3). This geometry puts the updip edge of the locked zone at a depth of 22 km, 46 km horizontal distance from the trench, and 51 km from the trench measured along the interface. The zone of pseudo-coupling around the locked area appears as an annulus of reduced slip magnitude on the plate interface. Note that when we describe model results, we refer to the magnitude of plate interface slip, which is related to the accumulation of slip deficit by

$$\text{slip deficit} = \text{relative plate motion} - \text{plate interface slip}$$

The functional shape of plate interface slip as it recovers to full plate motion is similar in the downdip and along-strike directions. Fault slip increases from zero at the edge of the locked zone to 0.5 m over a distance of ~20 km (measured along the fault). By ~70 km from the edge, slip is at 0.8 m, and by ~120 km from the edge, slip is back to 0.9 m, making it practically indistinguishable from the plate rate. The fault slip recovers more gradually updip of the locked zone because of the effects at shallow depths of the nearby free surface. As a result, the area of the megathrust between the updip edge of the locked patch and the trench does not slide at the relative plate motion rate despite being free to slide (similar to the result from Almeida et al., 2018). In the reference model, the magnitude of fault slip at the trench updip of the locked zone is 0.51 m.

3.1.2. Displacements

The relative motion of the subducting plate drives the upper plate toward the backstop (the positive x direction) and downward at the locked zone (the black arrows in Figure 4 show the displacements in a cross section through the reference model at y = 500 km). Upper plate displacements have the largest magnitudes (0.60–0.65 m) adjacent to and updip of the locked zone and decrease in magnitude with distance from the locked zone toward the backstop. The displacements along the surface of the upper plate are comparable to geodetic observations, such as those which are used to infer patterns of slip deficit accumulation. For the 1 m of relative motion and 25° dip in the reference model, the magnitude of the horizontal surface displacement is 0.38 m at the trench and increases slightly to its maximum value of 0.41 m above the updip edge of the locked zone (solid purple line in Figure 4, inset). The horizontal displacement decreases to 0.25 m above the downdip edge of the locked zone and further decreases with distance from the trench until it is zero at the backstop. Vertical surface displacements change more sharply with distance (solid green line in Figure 4, inset). At the trench, the upper plate subsides 0.23 m, and the maximum subsidence (0.35 m) occurs above the updip edge of the locked area. By the downdip edge of the locked zone, the magnitude of subsidence is 0.12 m, and the vertical motion is practically zero at distances of $\geq$150 km from the trench. Note that the reference model, which is completely elastic, produces only subsidence along the surface of the upper plate.

3.1.3. Stresses

We quantify the stress field in the plates around the locked zone with the principal stresses (arrows in Figure 5) and the potential for earthquake slip with the maximum shear stress (τ_{max}; color contours in Figure 5). The stress field in the upper plate is dominated by compression associated with horizontal shortening. The principal stresses in the subducting plate are also compressive at depths shallower than the downdip edge of the locked zone but become dominantly tensional at greater depths. The maximum shear stress τ_{max} (the second invariant of the deviatoric stress tensor) is largest near the edges of the locked zone, with a maximum value of 6.1 MPa in the reference model. τ_{max} decreases with distance from the locked zone until it is $\leq$0.1 MPa at distances of ~100 km or greater. Although τ_{max} is $\geq$0.25 MPa in the upper plate between updip edge of the locked zone and the trench, the dominant contribution to the stress tensor in this region is a large σ_{yy}

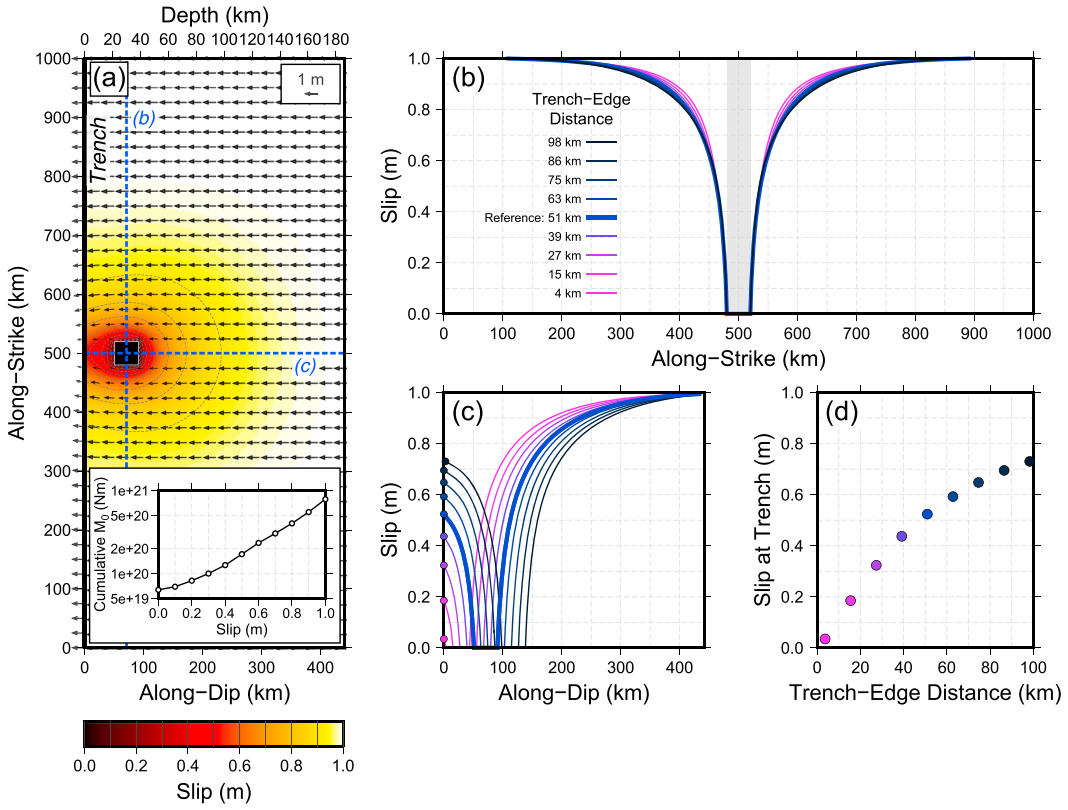

Figure 3. Plate interface slip in the reference model. (a) Slip distribution on the megathrust. The location of the locked zone is indicated by the white square. Colors indicate slip magnitude, from zero (black) to 1 m (white). Vectors show the motion of the upper plate relative to the subducting plate. The inset shows the seismic moment deficit accumulated within slip contours. Locations of fault slip transects are indicated by blue dashed lines. (b) Along-strike fault slip transect in the reference model (bold blue curve) and for the same locked zone at different depths (depth indicated by line color). The depth of the locked zone does not significantly change the along-strike pattern. (c) Along-dip fault slip transect for the locked zone at different depths. The reference model is indicated by the bold blue curve. (d) Slip at the trench versus along-dip distance between the trench and the edge of the locked zone.

component (supporting information Figure S1). Therefore, the part of the upper plate near the trench does not accumulate significant shear stress associated with megathrust earthquake slip (supporting information Figure S1f).

The shear tractions resolved onto the plate boundary (τ_{pb}) are responsible for driving coseismic slip in megathrust earthquakes (supporting information Figure S2). The spatial pattern primarily reflects the boundary conditions of the plate interface; outside the locked zone, τ_{pb} is zero, and inside the locked region, τ_{pb} is allowed to increase to arbitrarily high values to result in zero slip. The largest τ_{pb} on the megathrust accumulate along the interior edge of the locked zone, increasing asymptotically toward the edge (e.g., Okada, 1992). In the reference model, the maximum τ_{pb} is 4.1 MPa. In the middle of the locked region, τ_{pb} is lower, with a minimum value of 0.4 MPa.

3.1.4. Maximum Seismic Moment Deficit

Although the locked zone is responsible for building stresses toward the eventual earthquake, the reduced slip on the interface outside the locked zone is also slip deficit and can also potentially contribute to seismic moment release. The seismic moment deficit accumulated within the locked region in the reference model is $M_0 = 6.4 \times 10^{19}$ Nm (moment magnitude Mw 7.3), for a shear modulus of 40 GPa and 1 m of coseismic slip (Figure 3a, inset). Although the rate of seismic moment deficit accumulation per unit area is smaller in the regions of the model with reduced slip than in the locked zone, the total area accumulating moment deficit at a lower rate is large. In the context of our models, we cannot discriminate what percentage of this moment deficit would be released seismically. The maximum seismic moment accumulated over the entire megathrust in the reference model is 7.1×10^{20} Nm (Mw 7.9).

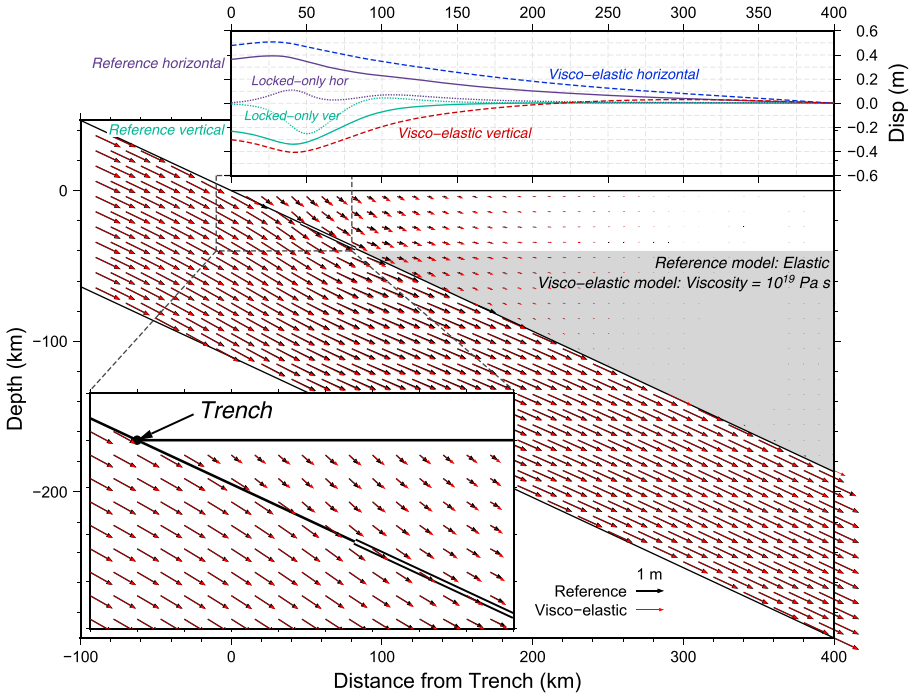

Figure 4. Modeled displacements projected onto a cross-section at $y = 500$ km. The location of the locked zone is indicated by a thick white line. The black displacement vectors are from the reference model, and the red vectors are from the viscoelastic model (the location of the viscoelastic region is shaded grey). Surface displacements along the upper plate are shown in the upper panel. The solid curves correspond to the reference model, the dashed lines are for the viscoelastic model, and dotted lines are from a single Okada (1992) fault coincident with the locked zone (ignoring slip elsewhere on the plate boundary). Note that the reference model produces only subsidence, whereas the viscoelastic model introduces flexure in the elastic region, causing subsidence near the trench and uplift near the backstop.

3.2. Sensitivity Tests

3.2.1. Sensitivity to Locked Patch Position

We evaluate how slip deficit at the trench depends on the location of the locked zone by shifting the updip edge of the locked patch updip and downdip relative to the reference model while keeping its dimensions the same (Figure 3). We test models with trench-edge distances (measured along the plate interface) ranging from 4 to 98 km. When the shallow limit of the locked zone is 4 km from the trench, only 0.03 m of slip occurs at the trench. Fault slip at the trench increases nearly linearly with locked zone distance up to approximately the position of the reference model (Figure 3d). Plate interface slip is more symmetric around locked zones deeper than the reference model because of less interaction with the free surface. Therefore, slip at the trench for these deeper locked zones simply follows the functional shape of reduced plate interface slip. Even a locked zone centered at the base of the seismogenic zone (50-km depth; trench-edge distance = 98 km) reduces the magnitude of slip at the trench to 0.72 m.

3.2.2. Sensitivity to Size of Square Locked Patch

We also explore the effects of varying the side length of the square locked patch from 10 to 80 km (supporting information Figure S3). To isolate this size-related effect from the position-related effect described in section 3.2.1, we fix the location of the shallow limit of the locked zone at the same position in these models (51 km from the trench, measured along the interface). Increasing the side length of the locked patch then moves the center and downdip edge of the locked zone farther from the trench. The magnitude of slip at the trench decreases with the increasing side length of the locked zone, from 0.78 m of slip for the 10 km locked region, to 0.51 for the 40-km locked region (the reference model), to 0.38 km for the 80 km locked zone. Over the rest of the interface along strike and downdip, larger locked zones result in larger areas with reduced slip, but this effect does not scale linearly with the size of the locked area. Smaller locked zones have a proportionally larger restrictive effect on the surrounding interface (as measured by the ratio of the size of the reduced slip area to the size of the locked region). Nevertheless, the broad regions of reduced slip around the largest locked zones will dominate the pattern of inter-seismic plate interface slip.

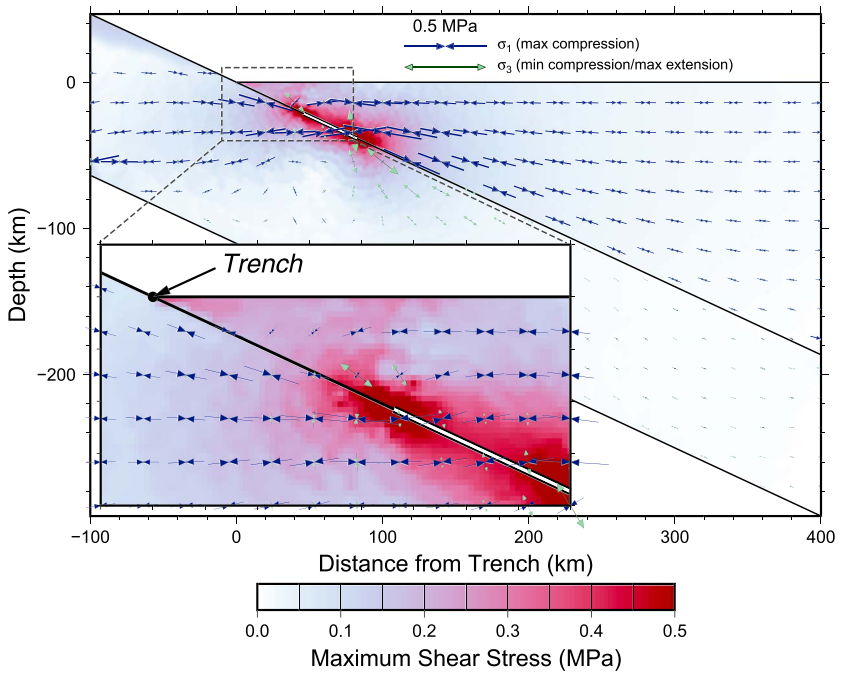

Figure 5. Stresses in the reference model projected onto a cross-section at $y = 500$ km. The background colors indicate the magnitude of the maximum shear stresses. The arrows show the orientations of principal stresses and are scaled by magnitude. The blue arrows indicate the maximum compressive stress, and the green arrows indicate the minimum compressive (or maximum tensional) stress.

3.2.3. Sensitivity to Dip of Plate Interface

Subduction zones typically have shallower dip angles near the trench, so we investigate how reducing the dip of the subducting plate affects the pattern of fault slip around the locked zone. We test models with dip angles ranging from 5° to 25°, while keeping the dimensions of the locked patch (40 km square) and the downdip distance between the trench and updip edge of the locked patch (51 km) the same as in the reference model. This test shows that the magnitude of fault slip updip of the locked zone is lower for shallower dip angles (supporting information Figure S4). At a dip angle of 5°, there is only 0.20 m of slip at the trench (compared to 0.51 m in the reference model). This effect is primarily a consequence of the thickness of the upper plate above the locked zone, which is defined by the subduction zone geometry. When this thickness is small (shallow dip), the near-trench region has relatively little mechanical connection to the rest of the upper plate, and therefore, its kinematics are more similar to that of the locked zone. As the dip angle and thickness increase, the region updip of the locked zone behaves less like the locked zone because it is more strongly connected to the rest of the upper plate. Downdip of the locked zone, the dip angle of the slab has relatively little effect on the pattern of fault slip.

3.2.4. Sensitivity to Along-Strike Length of Locked Patch

In many subduction zones, locked areas and associated earthquake slip extend much greater distances along strike ($>$200 km) than downdip (50–100 km; Figure 1). We test a model with a locked patch that is 250 km along strike (the "long-asperity model"), with all other aspects equal to the reference model. The long-asperity model shows reduced plate interface slip over a substantial area of the megathrust (Figure 6a). Updip of the locked zone, fault slip is 0.30 m at the trench (compared to 0.51 m in the reference model). Downdip of the locked zone, reduced slip extends close to the bottom edge of our modeled plate boundary. The extent of reduced slip along strike from the locked zone is short compared to the downdip extent, similar to that of the reference model.

The displacements on the surface of the upper plate in the long-asperity model also have a similar spatial pattern to those from the reference model but with greater magnitudes (Figure 6b). Near the trench, the upper plate moves 0.55 m toward the backstop and subsides 0.40 m. However, the upper plate within ~30 km horizontal distance of the trench has low τ_{max} ($<$0.05 MPa; Figure 6b), despite these large-magnitude surface

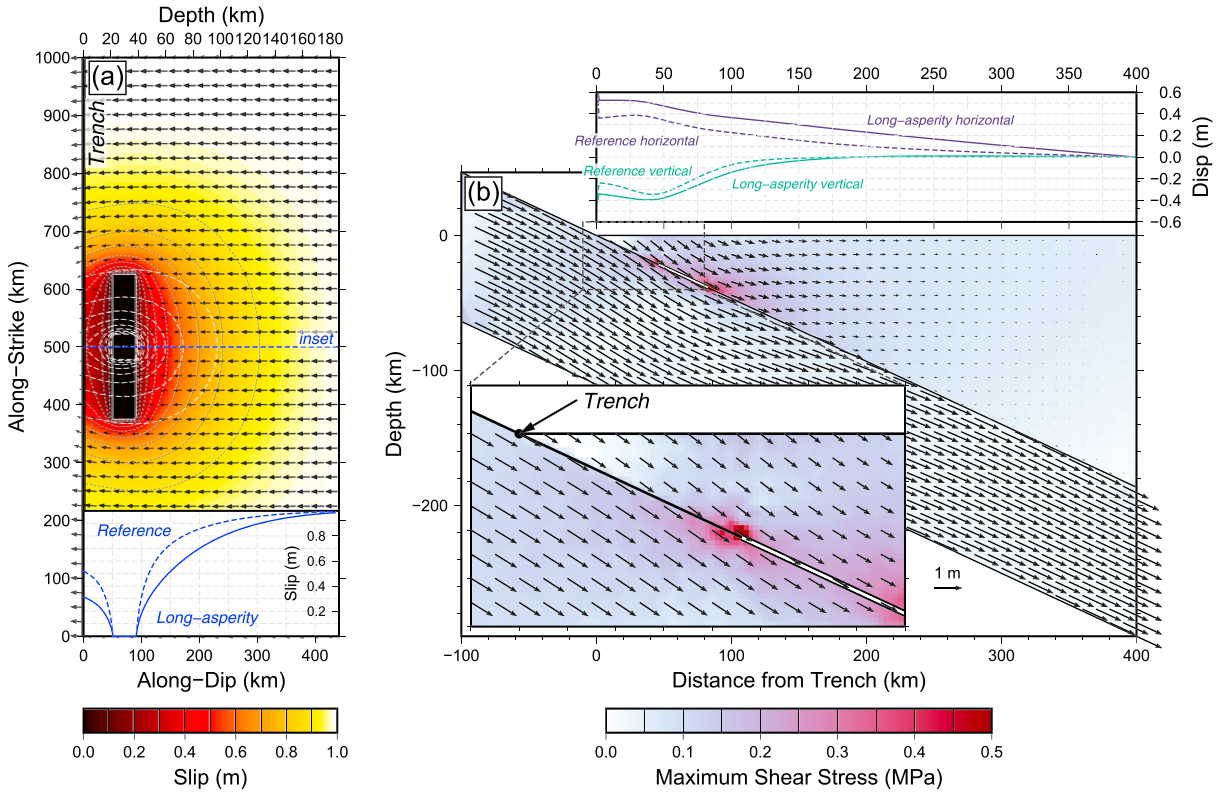

Figure 6. Results for the long-asperity model. (a) Fault slip, contoured the same as in Figure 3a. The white dashed lines show the 0.1-m slip contours from the reference model for comparison. The inset figure shows along-dip slip transects; the long-asperity model (solid line) has 0.3 m of slip near the trench and reduced slip extending farther downdip from the locked zone than in the reference model (dashed lines). (b) Cross section through the long-asperity model at y = 500 km showing maximum shear stresses as colors and displacements as vectors. Note the low magnitude of stress in the upper plate near the trench. Surface displacements for both the reference (dashed lines) and long-asperity (solid lines) models are plotted above the upper plate. The spatial pattern from the two models is similar, but the long-asperity model produces larger magnitude displacements.

displacements. This indicates that the part of the upper plate updip of the locked zone moves a large percentage of the plate motion and, importantly, it dominantly acts as a semirigid block, that is, without significant internal deformation.

3.2.5. Sensitivity to Asperity Strength

In previous models, the locked region had infinite strength, allowing the resistive shear tractions, τ_{pb}, to increase to arbitrarily high levels to keep the region from slipping. This is particularly relevant near the interior edge of the locked zone, where our reference model has τ_{pb} = 4.1 MPa and a completely locked fault has a shear stress singularity in analytical solutions (Okada, 1992). We test the effect of lowering τ_{pb} on the pattern of slip produced over the rest of the interface (supporting information Figure S2). This results in a small amount of fault slip inside the locked zone near the edges, thereby lowering the maximum magnitude of τ_{pb}. However, the pattern of reduced slip in unlocked regions around the locked zone does not change significantly when τ_{pb} is reduced near its edges.

3.2.6. Sensitivity to Shear Tractions in Unlocked Regions

The unlocked sections of the plate boundary can have nonzero sliding friction, so we investigate the effects of applying a uniform, constant shear traction of 0.3 MPa over these areas. The distribution of slip on the plate boundary for each 1 m of relative motion in this model is identical to that of the reference model. This pattern of fault slip also corresponds to identical accumulation of displacements, strains, and stresses throughout the model volume. The total stress field is the linear sum of the stress field from the reference model and the stress field corresponding to 0.3 MPa of shear traction applied outside the locked area. The only difference between this model and the reference model is this background stress level. This model indicates that the pseudo-coupling effect is insensitive to the magnitude of the shear traction on unlocked parts of the interface (even if the shear traction varies spatially), provided these tractions remain constant over time.

3.2.7. Sensitivity to Assumption of Purely Elastic Deformation

Over the timescales of interseismic loading, the thermal structure of the upper plate causes it to deform like an elastic sheet over a viscous fluid (Govers et al., 2018; Thatcher & Rundle, 1984). We investigate the sensitivity of our model results to this rheology by taking our reference model and assigning a Maxwell (linear) rheology with viscosity = 10^{19} Pa s in the upper plate at depths greater than 40 km (shaded region in Figure 4) to represent the behavior of the warmer, deeper lithosphere (the "viscoelastic model"). We examine the results after 100 one-year time steps with a relative motion rate of 1 cm/year, which allows the subjacent viscoelastic material to reach a loading steady state in response to the plate motion, then scale the results to match the kinematics of our reference model.

The pattern of reduced slip on the megathrust around the locked zone is similar to that of the reference model (supporting information Figure S5). Displacements in the upper plate are still oriented away from the trench but are ~15% larger in the viscoelastic model than in the reference model (Figure 4). Horizontal surface displacements are 0.49 m at the trench, 0.51 m above the updip edge of the locked zone, and decrease linearly from this maximum magnitude to zero at the backstop (blue dashed line in Figure 4, inset). All else remaining the same, the primary difference between the viscoelastic model and the reference model is in the vertical surface displacements. With this rheology, the upper plate acts as a relatively thin elastic sheet, which allows flexure in the elastic part of the plate. This results in 0.40 m of subsidence near the trench, which changes to slight uplift ~200 km from the trench (red dashed line in Figure 4, inset). The maximum uplift in this model is 0.05 m at 300 km from the trench. In contrast, the vertical displacements in the elastic-only model are uniformly downward. These models highlight how inferring plate interface slip with an elastic model can introduce substantial artifacts in the solution (e.g., Li et al., 2015). They also suggest that the artifacts are largest when using vertical motions, whereas the potential artifacts are smaller for the horizontal displacements.

3.3. Multiple Locked Zones

To quantify the importance of pseudo-coupling between adjacent asperities, we use a model configuration consisting of two locked patches from the reference model (the "two-asperity model"). We place these two 40-km square locked zones on the megathrust, centered at a depth of 30 km and separated along strike (Figure 7). When the two locked zones are 40 km (one side length) apart, the interface slip is similar to the slip produced by a single locked zone that is 120 km long (Figure 7b). The magnitude of fault slip in the intervening region is low, never exceeding 0.30 m, and the downdip extent of the reduced slip zone is expanded. As the locked zones become more separated, slip on the freely sliding interface between them increases (Figure 7a, inset) and the surface displacement footprint produced by each locked zone separates along strike (supporting information Figure S6). The reduction in interface slip between two locked zones is not a linear combination of the slip surrounding two individual locked zones, so the basic locking elements from the reference model along with its adjacent partial slip zones cannot be simplistically used as Green's functions in linear inversions. When the offset distance reaches 200 km (five side lengths), the slip in the midpoint between the two asperities is above 0.80 m (Figure 7d). Subduction megathrusts rarely seem to have creeping sections that extend more than 200 km along-strike (a notable exception is the Shumagin Gap in the Aleutians; Freymueller & Beavan, 1999), suggesting that most subduction zones will contain asperities with overlapping pseudo-coupled zones.

We also use the results from the two-asperity model to evaluate how much of the interseismic slip deficit accumulation in one asperity is taken up by the pseudo-coupling from its neighbor. When the two locked zones are separated by 40 km, the left asperity by itself reduces fault slip in the center of the right asperity to 0.76 m (Figure 7b, light blue area). Note that this is simply the result from the reference model at a distance of 60 km from the edge of the left asperity. Locking the right asperity reduces the fault slip from this pseudo-coupling level (0.76 m) to zero (dark red area). For greater separation distances, the proportion of locking in the right asperity that comes from the pseudo-coupling of the left locked zone decreases. For a separation distance of 120 km between the locked areas, pseudo-coupling accounts for 0.09 m out of the full 1 m in the right locked zone (Figure 7c). By a separation distance of 200 km, the level of pseudo-coupling in the right locked zone is only 0.02 m (Figure 7d), implying that nearly all the slip deficit accumulating in the right locked zone comes from it being locked, rather than from the influence of the left asperity.

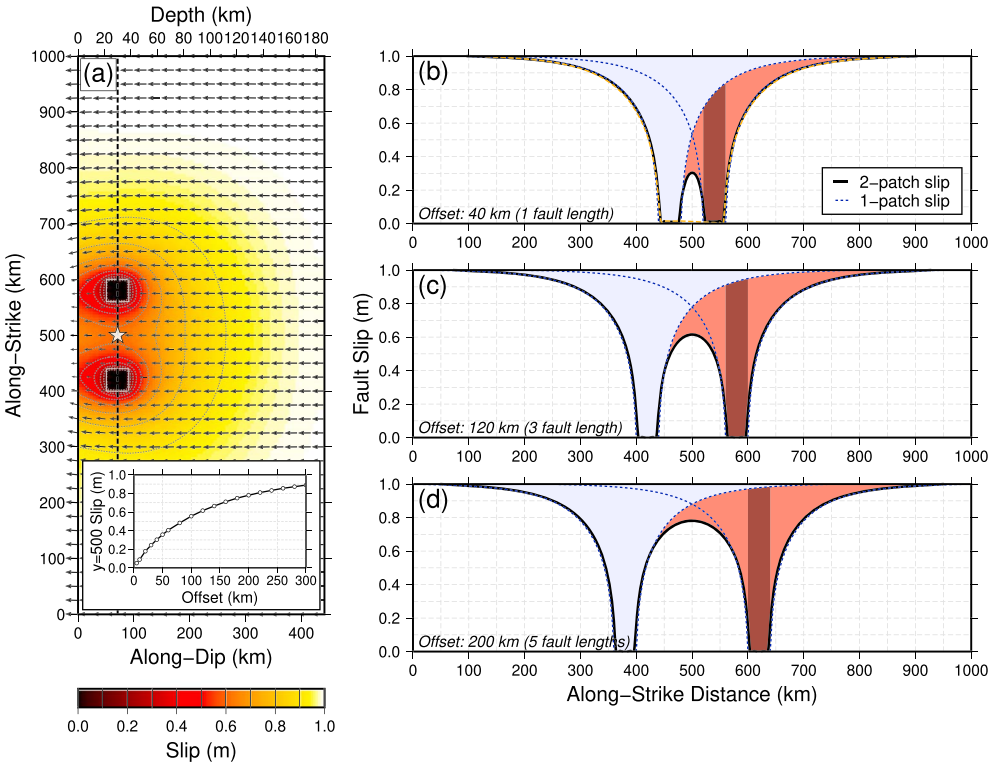

Figure 7. Plate interface slip in the two-asperity model. (a) Contours of fault slip around two 40 km square locked zones separated by 120 km, colored as in Figure 3a. The location of along-strike transects is indicated by the black dashed line. The inset figure shows the amount of interface slip at y = 500 km versus offset distance. (b) Slip transect for locked zones separated by 40 km. The bold black line indicates the fault slip resulting from both locked zones. The blue dashed lines indicate the fault slip generated by a single locked zone at the location of each asperity, without the effect of the other. The light red area indicates the maximum slip if only the right side asperity is unlocked. The dark red area indicates the maximum slip within the right asperity boundary. When the locked zones are close, they appear similar to one continuous, 120 km long locked section (orange dashed line). (c) As the gap between the locked zones increases (here shown 120 km apart), more slip occurs between them and they become distinguishable. (c) Once the asperities are far enough apart (here shown 200 km apart), they begin to behave more like independent locked zones, but their pseudo-coupling overlaps even at this separation distance.

3.3.1. Implications of Multiple Asperities for Coseismic Slip

If only one of the two locked areas ruptures, then that region cannot recover all of the slip deficit accumulated at that location. Even in the case of complete stress drop in the ruptured asperity, where, the shear traction goes to zero, our models show that there will still be slip deficit at that location because of the pseudo-coupling around the adjacent locked zone. In other words, only the portion of slip deficit in excess of the pseudo-coupling from adjacent locked asperities can be released coseismically. This means that as the distance between locked regions decreases, the maximum amount of coseismic slip that can occur in the rupture of a single asperity decreases according to the functional form of the pseudo-coupling of the unruptured locked zone. For example, in the case of two 40-km square locked regions separated by 40 km, the maximum amount of coseismic slip available to occur in the right asperity is ~75% of the plate motion (Figure 7b). In fact, the amount of slip available in this scenario varies over the length of the rupturing asperity; the side closest to its locked neighbor can slip 70% of the total accumulated slip deficit while the far side can slip up to 80%. This asymmetry is enhanced as the rupture area gets closer to the edge of the locked asperity.

We explicitly test the influence of pseudo-coupling and rupture length on the maximum possible magnitude of coseismic slip with a model consisting of three asperities (Figure 8). All three asperities have the same 40-km downdip extent as in the reference model. We evaluate the maximum coseismic slip for central asperity lengths of 40, 160, and 280 km. The two side asperities are each fixed at 200 km long, and the gap between the edges of the central asperity and the side asperities is set to 40 km. As in the reference model, we first accumulate interseismic slip deficit around the three locked asperities for 1 m of relative motion. We then

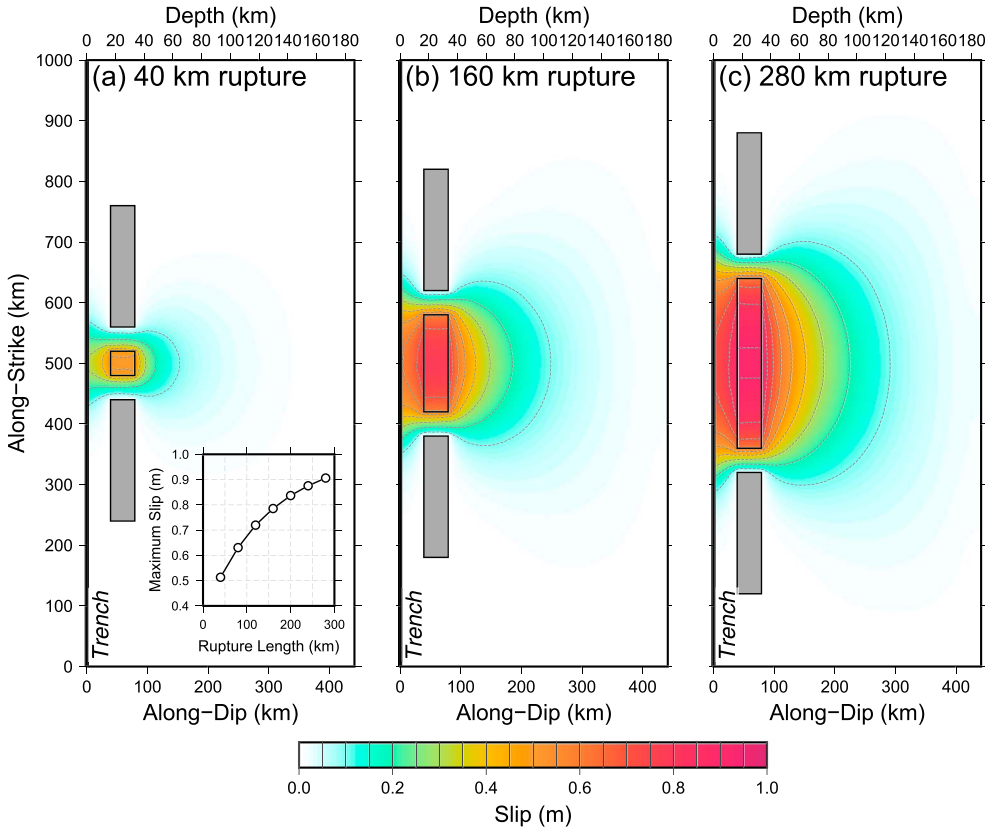

Figure 8. Maximum possible coseismic slip when an asperity is unlocked while adjacent asperities (shaded regions) remain locked. Maximum slip magnitude is contoured with colors. (a) In an earthquake the size of the reference model (40 km by 40 km), the maximum amount of slip that occurs is 0.50 m. The inset shows how the maximum slip magnitude increases with rupture length. (b) For a 160-km-long earthquake, the maximum slip is 0.75 m. (c) Once the earthquake exceeds a rupture length of ~250 km, it can release nearly the entire accumulated slip deficit in the parts of the rupture zone farthest from the adjacent locked asperities.

simulate the maximum possible slip in a rupture of the central asperity by unlocking it, while keeping the side asperities locked and other parts of the interface unlocked. This allows rebound to occur in both the central asperity and its surrounding pseudo-coupled zone. For a 40-km-long rupture, the maximum slip is 45% of the total accumulated slip deficit (Figure 8a). The amount of slip in the central asperity increases with rupture length. A typical Mw 8.0 earthquake has a length of 100–150 km (Allen & Hayes, 2017), which our models suggest can have a maximum coseismic slip of 60–75% of the total accumulated slip deficit. At a threshold rupture length of ~250 km the center of the rupture area is far enough from the pseudo-coupling zones of its locked neighbors that the earthquake can release almost the entire interseismic slip deficit. The peak co-seismic slip saturates at 1 m, and further growth of the rupture zone increases only the area that can slip this maximum amount (Figure 8c). This correlation between slip magnitude and rupture length also appears in other (dynamic) numerical models (e.g., Kaneko et al., 2010) as well as analog models of interacting asperities (e.g., Corbi et al., 2017). Note that because this model has identical locked asperities on either side of the rupture zone, the slip is symmetric. If the distribution and sizes of locked and unlocked regions were more complex, the asymmetry shown in Figure 7 could become visible in the co-seismic slip pattern as well.

4. Discussion

4.1. Comparison of Pseudo-coupling Models With Elastic Half-Space Models

We first evaluate whether a typical interseismic inversion method is compatible with the patterns of pseudo-coupling in our models. If we take the slip over the entire megathrust in the reference model and use it as the input in a back-slip model (Savage, 1983) with Green's functions for fault slip in an elastic half-space (Okada,

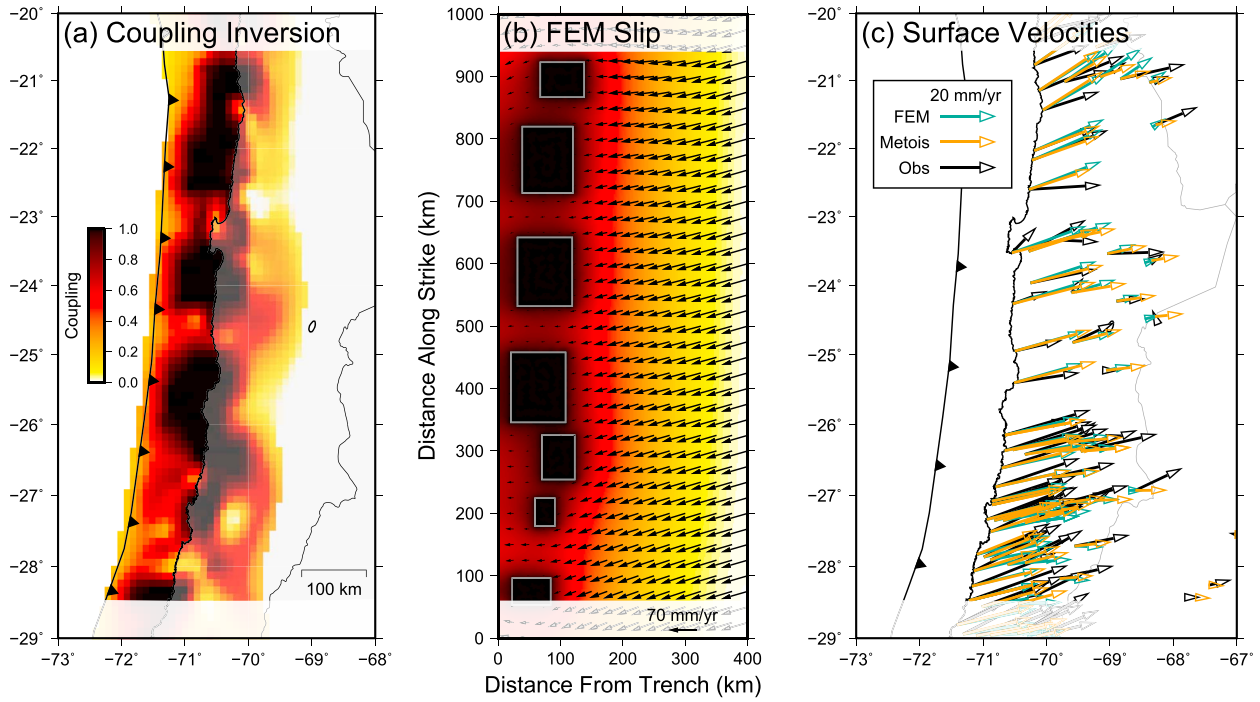

Figure 9. Comparison of fault slip and surface displacements between a pseudo-coupling model and an elastic half-space-based inversion (Metois et al., 2016). (a) Coupling distribution inverted from inter-seismic GPS velocities (black arrows in (c)). (b) Plate interface slip around seven locked zones in a pseudo-coupling model. These locked zones are areas with coupling values close to 1.0 identified in (a). Fault slip vectors are shown as black arrows. (c) Observed and synthetic horizontal surface velocities. Observed velocities are in black. Synthetic velocities from the Metois et al. (2016) coupling model shown in (a) are in orange. Synthetic velocities from the FEM corresponding to the fault slip distribution shown in (b) are in green. All of these horizontal surface velocities show a general agreement in both direction and magnitude.

1992), then the resulting displacement field is practically the same as in the reference model (supporting information Figure S7). This indicates that the displacement field depends on the fault slip over the whole plate boundary, irrespective of the mechanical coupling at each point (Wang & Dixon, 2004). An inversion of these displacements using the same Green's functions could recover the complete distribution of plate interface slip, assuming that the observations are distributed in a way that provides good resolution of the plate boundary. However, these inversions do not necessarily indicate specific interface frictional properties.

However, a limitation of this standard inversion procedure is that the fault segments have no inherent interactions between them. Therefore, areas inferred to be fully locked in this type of slip deficit inversion do not reduce the slip on the surrounding parts of the plate boundary. Some inversion regularization approaches (e.g., Laplacian smoothing) can approximate the interactions between adjacent sections of the interface, but these do not typically capture the details of how areas interact. This can lead to biased estimates of asperity locations and dimensions, the magnitude of slip deficit that accumulates near the trench (Almeida et al., 2018), the slip deficit downdip of the seismogenic zone, and the distribution of shear tractions.

We explore these differences further by comparing the patterns of fault slip and surface displacements predicted by a pseudo-coupling model to an inter-seismic GPS data set and slip deficit inversion for the South America subduction zone offshore Chile (Metois et al., 2016). That study applied a standard back-slip inversion approach with elastic half-space Green's functions and identified multiple regions interpreted to be accumulating full slip deficit, with lower inferred coupling between these fully locked regions (Figure 9a). In their slip deficit solution from 20°S to 29°S, we identify seven distinct locked zones surrounded by regions with apparent partial coupling (pseudo-coupling?; Figure 9b). We define these seven areas as locked in a pseudo-coupling model and assign the rest of the interface to have zero shear resistance. To better represent the geometry and kinematics of the South America subduction zone, the dip of the interface in this model is 20° and the convergence azimuth is 75°. The relative displacement is scaled to reflect one year of Nazca-South America motion (70 mm; DeMets et al., 2010). Because of the obliquity of the plate motion and asperities located near the along-strike edges in this model, there are significant interactions between the

pseudo-coupled regions and the side surfaces. Therefore, we do not use results within 60 km of the ends of the model.

The pseudo-coupling model produces a distribution of slip on the interface that resembles that of the inversion, even without precisely matching the interface geometry or plate kinematics of the system (cf., Figures 9a and 9b). In both models, there is low interseismic slip (high slip deficit accumulation; 50–90% of the relative plate motion) extending along strike between the fully locked asperities. The pseudo-coupling model also has low slip (high slip deficit; >60% of the convergent motion) up to the trench, whereas the half-space inversion puts less slip on the shallow interface (a region poorly resolved by onshore observations). Downdip of the locked asperities, the half-space inversion has an abrupt transition from fully locked to sliding at the relative plate velocity over a horizontal distance of ~50 km. In the pseudo-coupling model, this transition occurs over a much larger distance.

Despite the differences in the patterns of fault slip, the pseudo-coupling model produces horizontal surface velocities that are comparable in orientation and magnitude to the observed velocities, implying that it provides a reasonable explanation for this GPS data set (Figure 10c). The fit of the pseudo-coupling model horizontal surface velocities to observed velocities is similar to that of the synthetic velocities produced by the inverted slip deficit distribution. The vertical components of these GPS observations show that much of onshore Chile is uplifting at rates of up to 5 mm/year, while some coastal regions subside at several mm/year. Similar patterns of interseismic vertical motions (subsidence near the coast and uplift farther inland) are also observed in the subduction zones in Cascadia (Burgette et al., 2009), Japan (Aoki & Scholz, 2003), and Sumatra (Chlieh et al., 2008). Instead of fitting these vertical motion data sets with a sharp downdip transition from locked to sliding at the plate rate (as is done in many elastic half-space inversions), we attribute them to flexure of the elastic portion of the upper plate above its warmer, viscoelastic base (section 3.2.6; Figure 4).

4.2. Earthquake Implications

The slip deficit produced by pseudo-coupling of the plate interface limits the maximum possible slip if a neighboring asperity does not rupture. The Iquique section of the Chilean subduction zone provides a useful test of this hypothesis, because a large fraction of the slip deficit over much of the plate interface in this region was likely released in the last giant earthquake in 1877 (Mw ~ 8.8). From 1877 to 2014, no event larger than Mw 7.5 occurred in this section of the subduction zone (Kelleher, 1972; Lomnitz, 2004). The total interseismic slip deficit accumulated over this period was 9–10 m (at a convergence rate of 65–73 mm/year; Angermann et al., 1999; DeMets et al., 2010). For a rupture length of 100–150 km, the pseudo-coupling models in this study indicate that the coseismic slip can be up to 60–75% of the total slip deficit (5–7 m for the Iquique section; Figure 8). The 2014 Iquique earthquake had a rupture length of ~100 km and peak slip of 5–7 m (Figure 1a), consistent with these estimates. In other words, we interpret that the Iquique earthquake released nearly the maximum amount of coseismic slip deficit possible because of its closeness to a nonrupturing asperity. This still leaves 3–5 m of slip deficit on the region of the interface ruptured by the earthquake. Another effect of the Iquique earthquake is that the pseudo-coupling that was previously associated with the ruptured asperity may have disappeared. This pseudo-coupling would have reduced the maximum possible co-seismic slip on adjacent sections of the plate interface, but now that it is gone, subsequent events on asperities adjacent to the Iquique rupture zone can potentially have greater magnitude co-seismic slip.

The pre-earthquake slip deficit is more difficult to constrain for the Illapel section of the Chilean subduction zone, but the magnitude of coseismic slip in this event is also compatible with estimates from pseudo-coupling models. The region from 30 to 33°S last experienced a giant event in 1730 (Mw ~ 9.0) and since then has experienced at least four Mw 8.0–8.5 earthquakes (Kelleher, 1972; Lomnitz, 2004). The total convergence from 1730 to 2015 was ~21 m (at 74 mm/year), The 2015 earthquake had a rupture length of ~150 km, which corresponds to a maximum slip of 11–15 m in the pseudo-coupling model. Estimates of peak slip in the Illapel earthquake range from 7 to 12 m (Figure 1b). Despite the more complicated history of earthquakes in this part of the subduction zone, the coseismic slip is still compatible with the maximum amount allowed by adjacent locked asperities.

The very largest earthquakes, with rupture lengths >300 km, have coseismic slip that occurs far from adjacent locked asperities. These areas in the middle of large earthquake rupture zones can potentially slip

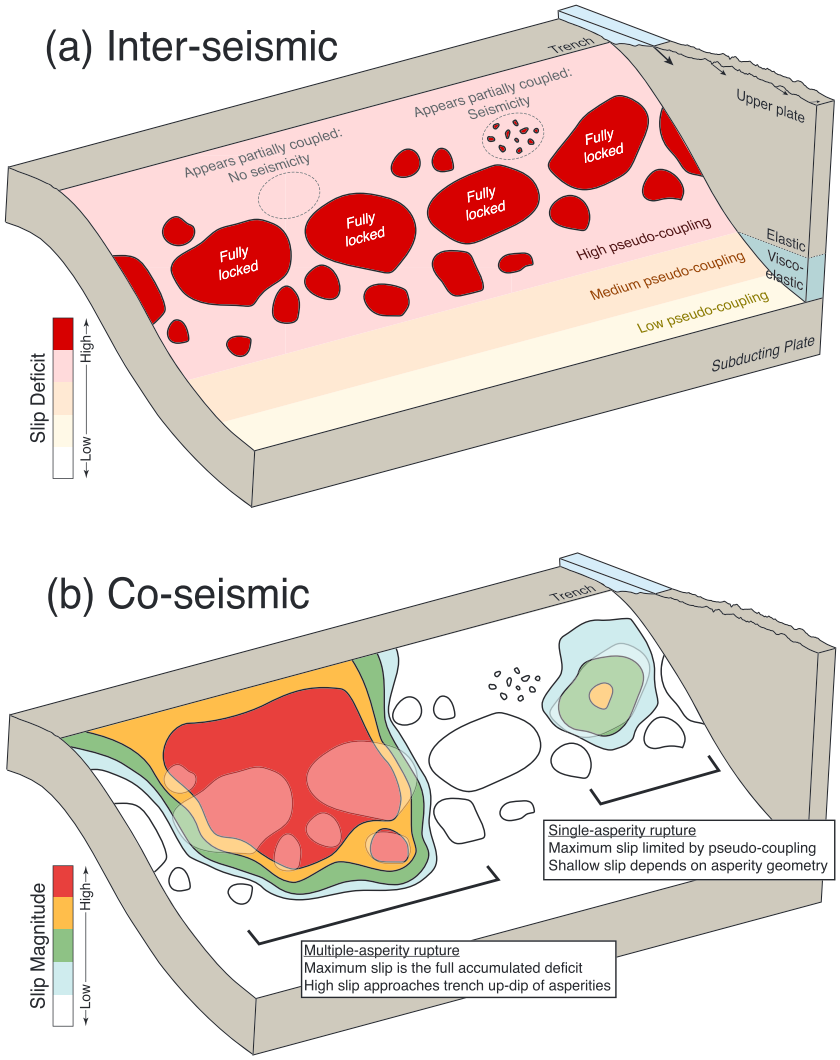

Figure 10. Synoptic picture of inter- and co-seismic slip on the subduction interface. (a) In between earthquakes, locked asperities of varying dimensions (dark red areas) accumulate slip deficit at or near the convergence rate. Near these asperities and updip of this region, slip deficit accumulates due to pseudo-coupling at a high fraction of the plate motion rate (light red areas). Downdip, the pseudo-coupling effect decreases until the plates move past each other at the full plate motion rate (orange to yellow areas). Regions that appear to have partial coupling may simply be pseudo-coupled and host little to no seismic activity, but small asperities on the interface in the pseudo-coupled region may appear also appear partially coupled (especially in the poorly resolved updip part of the interface) while still hosting seismicity. The rheology of the upper plate (elastic in the cooler, shallower regions and viscoelastic in the warmer, deeper regions) leads to flexure of the upper plate. (b) During an earthquake, the size of the rupture is a key factor in determining the magnitude of slip. Single asperity, smaller ruptures (right) have their slip reduced by pseudo-coupling generated by the neighboring asperities. These events may still produce shallow slip and tsunamis if the pseudo-coupling distribution relative to the rupture area allows shallow slip. In contrast, multi-asperity, larger ruptures (left) produce much greater magnitude slip throughout the rupture area far from adjacent asperity pseudo-coupling zones. These events can access the entire slip deficit updip of the locked zone, which may be a large fraction of the total accumulated slip deficit.

up to the total slip deficit accumulated on the plate interface (Figure 8c). In the case of the Maule section of the Chilean subduction zone, 13–14 m of slip deficit had accumulated since three great earthquakes occurred in 1822–1837 (Kelleher, 1972; Lomnitz, 2004). Peak slip in the 2010 Maule event was 12–16 m (Figure 1c), consistent with releasing nearly all of the accumulated slip deficit in this location.

Offshore of Japan, the last Mw ~ 9.0 earthquake occurred in 869 (Minoura et al., 2001), implying ~90 m of slip deficit accumulation for a Pacific-North America velocity of 80 mm/year (DeMets et al., 2010). Peak slip estimates for the 2011 Tohoku earthquake were 45–65 m (Lay, 2018) or 50–75% of this total accumulated slip

deficit estimate. Numerous earthquakes occurring within the Tohoku rupture area between 869 and 2011 (including Mw ~ 7.0 earthquakes every 20–30 years and Mw ~ 8.0 events occurring at least once per century; Hashimoto et al., 2009; Simons et al., 2011; Satake, 2015) may account for at least part of the difference. To account for the other 30–40 m of slip deficit, there would have to be 5–7 Mw 8.0 events, 11–16 Mw 7.5 events, or 30–40 Mw 7.0 earthquakes (Allen & Hayes, 2017), consistent with the number of events that occurred in the 1,142 years between giant earthquakes.

4.3. Tsunami Implications

Although onshore geodetic observations do not provide information about slip on the shallow megathrust, tsunamis generated by recent great earthquakes (e.g., in the 2004 Sumatra, Lay et al., 2005; 2010 Maule, Moreno et al., 2010; and 2011 Tohoku, Mori et al., 2011, events), widespread geological evidence of coseismic slip in the accretionary wedge sections of subduction décollements (Hubbard et al., 2015), and slip deficit modeling (Almeida et al., 2018; this study) suggest that large coseismic shallow slip is possible at many subduction zones globally. We compare results from the models in this study to observations from the tsunami source region of the 2011 Mw 9.0 Tohoku earthquake to explore the role of pseudo-coupling effects in tsunami-generation processes.

Significant coseismic slip in the 2011 Tohoku earthquake propagated close to the trench (Lay, 2018), producing the widespread tsunami. Slip inversions of the Tohoku earthquake based on observations sensitive to the near-trench motion, such as tsunami waves (Fujii et al., 2011; Grilli et al., 2012; Mori et al., 2011) and seafloor geodetic measurements (Iinuma et al., 2012; Sato et al., 2011), are generally consistent with shallow slip that is comparable to or larger in magnitude than the deeper slip. In contrast, models based on seismic or onshore geodetic observations tend to image the greatest moment release at slightly greater depths (~30 km) and reduced moment release up to the trench (Ammon et al., 2011; Ozawa et al., 2011; Simons et al., 2011; Yue & Lay, 2011). It should be noted that some inversions utilizing seismic or geodetic data sets do produce maximum slip at shallow levels; for example, reducing the shear modulus of the shallowest parts of the Earth model results in higher co-seismic slip estimates, overcoming the fact that relatively little seismic moment appears to be released in those locations (Hayes, 2011; Lay et al., 2011). Bathymetric changes indicated that the seafloor within 40 km of the trench shifted ~50 m eastward in the earthquake but moved without significant spatial gradients to the surface displacements (Fujiwara et al., 2011). Finally, postseismic borehole heat flow measurements showed a very small increase in temperature associated with coseismic frictional sliding, implying little change in shear traction during the earthquake in that area (Fulton et al., 2013).

A model of a subduction zone with a low-shear-resistance shallow megathrust updip of a broadly locked seismogenic zone produces results that provide a reasonable interpretation of these observations of the Tohoku earthquake, namely, (a) large amounts of shallow slip that (b) produced relatively weak seismic radiation; (c) block displacements of the upper plate near the trench; and (d) low coseismic heat production on the shallow megathrust. In the long-asperity model, slip deficit at the trench is 0.70 m and the upper plate within 50 km of the trench displaces up to 0.65 m parallel to plate motion. These modeled interseismic displacements indicate the potential for significant shallow coseismic slip and corresponding static surface displacements. However, these large displacements are accompanied by low strain/stress accumulation in the upper plate within 30 km of the trench; in other words, this region moves dominantly as a semirigid block (Figure 6). Because large-amplitude seismic waves are generated primarily by the release of elastic strain energy from rocks adjacent to the rupturing fault (Aki & Richards, 2002), this region accumulating little interseismic elastic strain should not be expected to release as much strain energy in an earthquake as the high strain regions near the locked asperity. Finally, if we assume that the shallow interface in this scenario has a similarly low shear resistance prior to and during the earthquake (Ujiie et al., 2013), the large-magnitude coseismic slip in this region would not produce significant heating due to sliding.

This coseismic slip on the shallow interface also implies that the mechanical interpretation of stress drop in pseudo-coupled areas is not as straightforward as for asperities. Within the asperity, the stress drop has a simple mechanical meaning: the difference in shear stress resolved onto the megathrust before and after the earthquake (Kanamori & Anderson, 1975). In contrast, pseudo-coupled sections of the interface have constant shear stress resolved on them prior to and following the earthquake (in our models). This means that despite potentially rupturing and hosting significant slip during the earthquake, the shear stress resolved

onto the ruptured sections of the plate boundary outside the asperity immediately after the earthquake may simply remain at a similar level from before the event.

5. Conclusions

The combination of interseismic and coseismic observations along with the results from our numerical models allows us to draw a synoptic picture of slip on the subduction plate interface prior to and during great earthquakes (Figure 10). Asperities are concentrated at depths of 10–50 km, in the seismogenic zone, and can take on a range of sizes. During the interseismic period, the interface within these asperities accumulates slip deficit at or near 100% of the plate convergence rate (Figure 10a). The interface immediately adjacent to the asperities has high levels of pseudo-coupling, accumulating slip deficit at a large fraction of the convergence rate. Up-dip of the seismogenic zone there are fewer asperities, so there is little to no seismicity. In this part of the plate boundary, high, uniform slip deficit accumulates due to pseudo-coupling and the narrowing thickness of the upper plate. Some apparently partially coupled regions on the interface may host some smaller magnitude seismicity; we interpret these regions to contain small asperities that cannot be resolved by current imaging techniques. Downdip of the asperities, the pseudo-coupling decays until the plates move past each other at the full rate.

In the ensuing earthquake, the coseismic slip behavior depends largely on whether one or multiple asperities slip. In a single-asperity rupture, the maximum slip can be up to the pseudo-coupling level of the neighboring asperities, implying smaller peak slip magnitudes (Figure 10b). Our modeling results suggest that shallow slip may depend on the location of the slipping asperity and the distribution of unruptured asperities around the rupture, which limit the magnitude of any shallow slip. Once a rupture is sufficiently long (our models suggest a length of ~250 km or more), the pseudo-coupling produced by adjacent asperities in the middle of the slipping asperities drops to essentially zero, so the earthquake can have a maximum slip that is nearly the entire accumulated deficit. This accounts for the much greater slip values in earthquakes with larger rupture lengths. These observations are reflected in patterns of coseismic slip seen in recent great earthquakes. If the shallow part of the plate boundary updip of the rupture zone can slip along with the deeper asperity, this region may slip up to its total accumulated pseudo-coupling level, which our models demonstrated are ~75% of the total slip deficit. This results in substantial motion of the seafloor and a large tsunami, without necessarily generating the characteristic seismic waves and heat generation typically expected for slip in typical asperities.

Acknowledgments

This work was supported by NASA Earth and Space Science Fellowship NNX14AL21H. Many of the figures in this manuscript were created using the Generic Mapping Tools (Wessel & Smith, 1991). We thank J. Loveless and an anonymous reviewer for comments that helped to improve the manuscript. Seismic, geodetic, and other observational data sets can be found in their cited sources. The reference model geometry file and finite element model output files are available in the supporting information.

References

Aki, K., & Richards, P. G. (2002). *Quantitative seismology*. Sausalito, CA: University Science Books.

Allen, T. I., & Hayes, G. P. (2017). Alternative rupture-scaling relationships for subduction interface and other offshore environments. *Bulletin of the Seismological Society of America*, *107*(3), 1240–1253. https://doi.org/10.1785/0120160255

Almeida, R., Lindsey, E. O., Bradley, K., Hubbard, J., Mallick, R., & Hill, E. M. (2018). Can the updip limit of frictional locking on megathrusts be detected geodetically? Quantifying the effect of stress shadows on near-trench coupling. *Geophysical Research Letters*, *45*, 4754–4763. https://doi.org/10.1029/2018GL077785

Ammon, C. J., Lay, T., Kanamori, H., & Cleveland, M. (2011). A rupture model of the 2011 off the Pacific coast of Tohoku earthquake. *Earth, Planets and Space*, *63*(7), 693–696. https://doi.org/10.5047/eps.2011.05.015

Angermann, D., Klotz, J., & Reigber, C. (1999). Space-geodetic estimation of the Nazca-South America Euler vector. *Earth and Panetary Science Letters*, *171*(3), 329–334. https://doi.org/10.1016/S0012-821X(99)00173-9

Aoki, Y., & Scholz, C. H. (2003). Vertical deformation of the Japanese islands, 1996–1999. *Journal of Geophysical Research*, *108*(B5), 2257. https://doi.org/10.1029/2002JB002129

Audet, P., Bostock, M. G., Christensen, N. I., & Peacock, S. M. (2009). Seismic evidence for overpressured subducted oceanic crust and megathrust fault sealing. *Nature*, *457*(7225), 76–78. https://doi.org/10.1038/nature07650

Avouac, J. P. (2015). From geodetic imaging of seismic and aseismic fault slip to dynamic modeling of the seismic cycle. *Annual Review of Earth and Planetary Sciences*, *43*(1), 233–271. https://doi.org/10.1146/annurev-earth-060614-105302

Burgette, R. J., Weldon, R. J. II, & Schmidt, D. A. (2009). Interseismic uplift rates for western Oregon and along-strike variation in locking on the Cascadia subduction zone. *Journal of Geophysical Research*, *114*, B01408. https://doi.org/10.1029/2008JB005679

Bürgmann, R., Kogan, M. G., Steblov, G. M., Hilley, G., Levin, V. E., & Apel, E. (2005). Interseismic coupling and asperity distribution along the Kamchatka subduction zone. *Journal of Geophysical Research*, *110*, B07405. https://doi.org/10.1029/2005JB003648

Chlieh, M., Avouac, J. P., Sieh, K., Natawidjaja, D. H., & Galetzka, J. (2008). Heterogeneous coupling of the Sumatran megathrust constrained by geodetic and paleogeodetic measurements. *Journal of Geophysical Research*, *113*, B05305. https://doi.org/10.1029/2007JB004981

Corbi, F., Funiciello, F., Brizzi, S., Lallemand, S., & Rosenau, M. (2017). Control of asperities size and spacing on seismic behavior of subduction megathrusts. *Geophysical Research Letters*, *44*, 8227–8235. https://doi.org/10.1002/2017GL074182

DeMets, C., Gordon, R. G., & Argus, D. F. (2010). Geologically current plate motions. *Geophysical Journal International*, *181*(1), 1–80. https://doi.org/10.1111/j.1365-246X.2009.04491.x

Freymueller, J. T., & Beavan, J. (1999). Absence of strain accumulation in the western shumagin segment of the Alaska subduction zone. *Geophysical Research Letters*, *26*(21), 3233–3236. https://doi.org/10.1029/1999GL008356
Fujii, Y., Satake, K., Sakai, S., Shinohara, M., & Kanazawa, T. (2011). Tsunami source of the 2011 off the Pacific coast of Tohoku earthquake. *Earth, Planets and Space*, *63*(7), 815–820. https://doi.org/10.5047/eps.2011.06.010
Fujiwara, T., Kodaira, S., No, T., & Kaiho, Y. (2011). The 2011 Tohoku-Oki earthquake: Displacement reaching the trench axis. *Science*, *332*(6036), 1426–1429. https://doi.org/10.1126/science.1207020
Fulton, P. M., Brodsky, E. E., Kano, Y., Mori, J., Chester, F., Ishikawa, T., et al. (2013). Low coseismic friction on the Tohoku-Oki fault determined from temperature measurements. *Science*, *342*(6163), 1214–1217. https://doi.org/10.1126/science.1243641
Gans, C. R., Furlong, K. P., & Malservisi, R. (2003). Fault creep and microseismicity on the Hayward fault, California: Implications for asperity size. *Geophysical Research Letters*, *30*(19), 2000. https://doi.org/10.1029/2003GL017904
Gao, X., & Wang, K. (2014). Strength of stick-slip and creeping subduction megathrusts from heat flow observations. *Science*, *345*(6200), 1038–1041. https://doi.org/10.1126/science.1255487
Geuzaine, C., & Remacle, J.-F. (2009). Gmsh: A 3-D finite element mesh generator with built-in pre- and post-processing facilities. *International Journal for Numerical Methods in Engineering*, *79*(11), 1309–1331. https://doi.org/10.1002/nme.2579
Govers, R., Furlong, K. P., van de Wiel, L., Herman, M. W., & Broerse, T. (2018). The geodetic signature of the earthquake cycle at subduction zones: Model constraints on the deep processes. *Reviews of Geophysics*, *56*, 6–49. https://doi.org/10.1002/2017RG000586
Govers, R., & Wortel, M. J. R. (1993). Initiation of asymmetric extension in continental lithosphere. *Tectonophysics*, *223*(1-2), 75–96. https://doi.org/10.1016/0040-1951(93)90159-H
Govers, R., & Wortel, M. J. R. (2005). Lithosphere tearing at STEP faults: Response to edges of subduction zones. *Earth and Planetary Science Letters*, *236*(1–2), 505–523. https://doi.org/10.1016/j.epsl.2005.03.022
Grilli, S. T., Harris, J. C., Tajalli Bakhsh, T. S., Masterlark, T. L., Kyriakopoulos, C., Kirby, J. T., & Shi, F. (2012). Numerical simulation of the 2011 Tohoku tsunami based on a new transient FEM co-seismic source: Comparison to far- and near-field observations. *Pure and Applied Geophysics*, *170*(6–8), 1333–1359. https://doi.org/10.1007/s00024-012-0528-y
Hardebeck, J. L. (2015). Stress orientations in subduction zones and the strength of subduction megathrust faults. *Science*, *349*(6253), 1208–1213. https://doi.org/10.1126/science.aac8343
Hardebeck, J. L., & Loveless, J. P. (2017). Creeping subduction zones are weaker than locked subduction zones. *Nature Geoscience*, *11*(1), 60–64. https://doi.org/10.1038/s41561-017-0032-1
Hashimoto, C., Fukuyama, E., & Matsuura, M. (2014). Physics-based 3-D simulation for earthquake generation cycles at plate interfaces in subduction zones. *Pure and Applied Geophysics*, *171*(8), 1705–1728. https://doi.org/10.1007/s00024-013-0716-4
Hashimoto, C., Noda, A., Sagiya, T., & Matsuura, M. (2009). Interplate seismogenic zones along the Kuril-Japan trench inferred from GPS data inversion. *Nature Geoscience*, *2*(2), 141–144. https://doi.org/10.1038/ngeo421
Hayes, G. P. (2011). Rapid source characterization of the 2011 Mw 9.0 off the Pacific coast of Tohoku earthquake. *Earth, Planets and Space*, *63*(7), 529–534. https://doi.org/10.5047/eps.2011.05.012
Hayes, G. P. (2017). The finite, kinematic rupture properties of great-sized earthquakes since 1990. *Earth and Planetary Science Letters*, *468*, 94–100. https://doi.org/10.1016/j.epsl.2017.04.003
Hayes, G. P., Wald, D. J., & Johnson, R. L. (2012). Slab1.0: A three-dimensional model of global subduction zone geometries. *Journal of Geophysical Research*, *117*, B01302. https://doi.org/10.1029/2011JB008524
Hetland, E. A., & Simons, M. (2010). Post-seismic and interseismic fault creep II: Transient creep and interseismic stress shadows on megathrusts. *Geophysical Journal International*, *181*(1), 99–112. https://doi.org/10.1111/j.1365-246X.2009.04482.x
Hubbard, J., Barbot, S., Hill, E. M., & Tapponnier, P. (2015). Coseismic slip on shallow décollement megathrusts: Implications for seismic and tsunami hazard. *Earth-Science Reviews*, *141*, 45–55. https://doi.org/10.1016/j.earscirev.2014.11.003
Hyndman, R. D., Yamano, M., & Oleskevich, D. A. (1997). The seismogenic zone of subduction thrust faults. *Island Arc*, *6*(3), 244–260. https://doi.org/10.1111/j.1440-1738.1997.tb00175.x
Ide, S., & Beroza, G. C. (2001). Does apparent stress vary with earthquake size. *Geophysical Research Letters*, *28*(17), 3349–3352. https://doi.org/10.1029/2001GL013106
Iinuma, T., Hino, R., Kido, M., Inazu, D., Osada, Y., Ito, Y., et al. (2012). Coseismic slip distribution of the 2011 off the Pacific Coast of Tohoku Earthquake (M9.0) refined by means of seafloor geodetic data. *Journal of Geophysical Research*, *117*, B07409. https://doi.org/10.1029/2012JB009186
Ikari, M. J., Marone, C., & Saffer, D. M. (2011). On the relation between fault strength and frictional stability. *Geology*, *39*(1), 83–86. https://doi.org/10.1130/G31416.1
Kanamori, H., & Anderson, D. L. (1975). Theoretical basis of some empirical relations in seismology. *Bulletin of the Seismological Society of America*, *65*(5), 1073–1095.
Kaneko, Y., Avouac, J. P., & Lapusta, N. (2010). Towards inferring earthquake patterns from geodetic observations of interseismic coupling. *Nature Geoscience*, *3*(5), 363–369. https://doi.org/10.1038/ngeo843
Kelleher, J. A. (1972). Rupture zones of large South American earthquakes and some predictions. *Journal of Geophysical Research*, *77*(11), 2087–2103. https://doi.org/10.1029/JB077i011p02087
Lay, T. (2018). A review of the rupture characteristics of the 2011 Tohoku-oki Mw 9.1 earthquake. *Tectonophysics*, *733*, 4–36. https://doi.org/10.1016/j.tecto.2017.09.022
Lay, T., Ammon, C. J., Kanamori, H., Xue, L., & Kim, M. J. (2011). Possible large near-trench slip during the 2011 M (w) 9.0 off the Pacific coast of Tohoku earthquake. *Earth, Planets and Space*, *63*(7), 687–692. https://doi.org/10.5047/eps.2011.05.033
Lay, T., Kanamori, H., Ammon, C. J., Koper, K. D., Hutko, A. R., Ye, L., et al. (2012). Depth-varying rupture properties of subduction zone megathrust faults. *Journal of Geophysical Research*, *117*, B04311. https://doi.org/10.1029/2011JB009133
Lay, T., Kanamori, H., Ammon, C. J., Nettles, M., Ward, S. N., Aster, R. C., et al. (2005). The great Sumatra-Andaman earthquake of 26 December 2004. *Science*, *308*(5725), 1127–1133. https://doi.org/10.1126/science.1112250
Li, S., Moreno, M., Bedford, J., Rosenau, M., & Oncken, O. (2015). Revisiting viscoelastic effects on interseismic deformation and locking degree: A case study of the Peru-North Chile subduction zone. *Journal of Geophysical Research*, *120*, 4522–4538. https://doi.org/10.1002/2015JB011903
Liu, Y., & Rice, J. R. (2005). Aseismic slip transients emerge spontaneously in three-dimensional rate and state modeling of subduction earthquake sequences. *Journal of Geophysical Research*, *110*, B08307. https://doi.org/10.1029/2004JB003424
Lomnitz, C. (2004). Major earthquakes of Chile: A historical survey, 1535–1960. *Seismological Research Letters*, *75*(3), 368–378. https://doi.org/10.1785/gssrl.75.3.368
Loveless, J. P., & Meade, B. J. (2011). Spatial correlation of interseismic coupling and coseismic rupture extent of the 2011 Mw = 9.0 Tohoku-oki earthquake. *Geophysical Research Letters*, *38*, L17306. https://doi.org/10.1029/2011GL048561

Mai, P. M., & Beroza, G. C. (2000). Source scaling properties from finite-fault-rupture models. *Bulletin of the Seismological Society of America*, *90*(3), 604–615. https://doi.org/10.1785/0119990126

Malservisi, R., Gans, C., & Furlong, K. P. (2003). Numerical modeling of strike-slip creeping faults and implications for the Hayward fault, California. *Tectonophysics*, *361*(1–2), 121–137. https://doi.org/10.1016/S0040-1951(02)00587-5

Melosh, H. J., & Williams, C. A. (1989). Mechanics of graben formation in crustal rocks: A finite element analysis. *Journal of Geophysical Research*, *94*(B10), 13,961–13,973. https://doi.org/10.1029/JB094iB10p13961

Metois, M., Vigny, C., & Socquet, A. (2016). Interseismic coupling, megathrust earthquakes and seismic swarms along the Chilean Subduction Zone (38°–18°S). *Pure and Applied Geophysics*, *173*(5), 1431–1449. https://doi.org/10.1007/s00024-016-1280-5

Minoura, K., Imamura, F., Sugawara, D., Kono, Y., & Iwashita, T. (2001). The 869 Jogan tsunami deposit and recurrence interval of large-scale tsunami on the Pacific coast of northeast Japan. *Journal of Natural Disaster Science*, *23*(2), 83–88.

Moreno, M., Rosenau, M., & Oncken, O. (2010). 2010 Maule earthquake slip correlates with pre-seismic locking of Andean subduction zone. *Nature*, *467*(7312), 198–202. https://doi.org/10.1038/nature09349

Mori, N., Takahashi, T., Yasuda, T., & Yanagisawa, H. (2011). Survey of 2011 Tohoku earthquake tsunami inundation and run-up. *Geophysical Research Letters*, *38*, L00G14. https://doi.org/10.1029/2011GL049210

Okada, Y. (1992). Internal deformation due to shear and tensile faults in a half-space. *Bulletin of the Seismological Society of America*, *82*, 1018–1040.

Ozawa, S., Nishimura, T., Suito, H., Kobayashi, T., Tobita, M., & Imakiire, T. (2011). Coseismic and postseismic slip of the 2011 magnitude-9 Tohoku-Oki earthquake. *Nature*, *475*(7356), 373–376. https://doi.org/10.1038/nature10227

Pacheco, J. F., Sykes, L. R., & Scholz, C. H. (1993). Nature of seismic coupling along simple plate boundaries of the subduction type. *Journal of Geophysical Research*, *98*(B8), 14,133–14,159. https://doi.org/10.1029/93JB00349

Saffer, D. M., & Marone, C. (2003). Comparison of smectite-and illite-rich gouge frictional properties: Application to the updip limit of the seismogenic zone along subduction megathrusts. *Earth and Planetary Science Letters*, *215*(1-2), 219–235. https://doi.org/10.1016/S0012-821X(03)00424-2

Satake, K. (2015). Geological and historical evidence of irregular recurrent earthquakes in Japan. *Philosophical Transactions of the Royal Society of London. Series A*, *373*(2053), 20140375. https://doi.org/10.1098/rsta.2014.0375

Sato, M., Ishikawa, T., Ujihara, N., Yoshida, S., Fujita, M., Mochizuki, M., & Asada, A. (2011). Displacement above the hypocenter of the 2011 Tohoku-Oki earthquake. *Science*, *332*(6036), 1395–1395. https://doi.org/10.1126/science.1207401

Savage, J. C. (1983). A dislocation model of strain accumulation and release at a subduction zone. *Journal of Geophysical Research*, *88*(B6), 4984–4996. https://doi.org/10.1029/JB088iB06p04984

Scholz, C. H. (1998). Earthquakes and friction laws. *Nature*, *391*(6662), 37–42. https://doi.org/10.1038/34097

Simons, M., Minson, S. E., Sladen, A., Ortega, F., Jiang, J., Owen, S. E., et al. (2011). The 2011 magnitude 9.0 Tohoku-Oki earthquake: Mosaicking the megathrust from seconds to centuries. *Science*, *332*(6036), 1421–1425. https://doi.org/10.1126/science.1206731

Thatcher, W., & Rundle, J. B. (1984). A viscoelastic coupling model for the cyclic deformation due to periodically repeated earthquakes at subduction zones. *Journal of Geophysical Research*, *89*(B9), 7631–7640. https://doi.org/10.1029/JB089iB09p07631

Thomas, M. Y., Lapusta, N., Noda, H., & Avouac, J. P. (2014). Quasi-dynamic versus fully dynamic simulations of earthquakes and aseismic slip with and without enhanced coseismic weakening. *Journal of Geophysical Research*, *119*, 1986–2004. https://doi.org/10.1002/2013JB010615

Tichelaar, B. W., & Ruff, L. J. (1993). Depth of seismic coupling along subduction zones. *Journal of Geophysical Research*, *98*(B2), 2017–2037. https://doi.org/10.1029/92JB02045

Turcotte, D. L., & Schubert, G. (2002). *Geodynamics*. Cambridge: Cambridge University Press. https://doi.org/10.1017/CBO9780511807442

Ujiie, K., Tanaka, H., Saito, T., Tsutsumi, A., Mori, J. J., Kameda, J., et al. (2013). Low coseismic shear stress on the Tohoku-Oki megathrust determined from laboratory experiments. *Science*, *342*(6163), 1211–1214. https://doi.org/10.1126/science.1243485

van Dinther, Y., Gerya, T. V., & Dalguer, L. A. (2013). The seismic cycle at subduction thrusts: Insights from seismo-thermo-mechanical models. *Journal of Geophysical Research: Solid Earth*, *118*, 6183–6202. https://doi.org/10.1002/2013JB010380

van Keken, P. E., Kiefer, B., & Peacock, S. M. (2002). High-resolution models of subduction zones: Implications for mineral dehydration reactions and the transport of water into the deep mantle. *Geochemistry, Geophysics, Geosystems*, *3*(10), 1056. https://doi.org/10.1029/2001GC000256

Wang, K., & Bilek, S. L. (2014). Invited review paper: Fault creep caused by subduction of rough seafloor relief. *Tectonophysics*, *610*, 1–24. https://doi.org/10.1016/j.tecto.2013.11.024

Wang, K., & Dixon, T. (2004). "Coupling" semantics and science in earthquake research. *Journal of Geophysical Research*, *108*(81), 2009. https://doi.org/10.1029/2001JB001227

Wessel, P., & Smith, W. H. F. (1991). Free software helps map and display data. *Eos, Transactions American Geophysical Union*, *72*(41), 441–446. https://doi.org/10.1029/90EO00319

Yue, H., & Lay, T. (2011). Inversion of high-rate (1 sps) GPS data for rupture process of the 11 March 2011 Tohoku earthquake (Mw 9.1). *Geophysical Research Letters*, *38*, L00G09. https://doi.org/10.1029/2011GL048700